Journal of Power Sources 266 (2014) 422–432

Contents lists available at ScienceDirect

Journal of Power Sources

journal homepage: www.elsevier.com/locate/jpowsour

An investigation on the significance of reversible heat to the thermal behavior of lithium ion battery through simulations

Rui Zhao, Junjie Gu, Jie Liu*

Department of Mechanical and Aerospace Engineering, Carleton University, Ottawa, ON K1S 5B6, Canada

HIGHLIGHTS

- The significance of reversible heat (RH) is analyzed in a Li-ion battery model.
- RH is important in thin electrode cell and in small solid particle cell.
- Thin electrode cell and fine solid particle cell exhibit good thermal performance.
- A correction diagram is proposed to modify the results of RH exclusive models.
- RH is non-ignorable for battery discharged at 10 C or lower rates.

ARTICLE INFO

Article history:
Received 11 March 2014
Received in revised form
9 May 2014
Accepted 10 May 2014
Available online 20 May 2014

Keywords:
Reversible heat
Li-ion battery
Coupling model
Heat generation
Electrode thickness
Active material particle size

ABSTRACT

As a typical heat source in the operation of lithium-ion (Li-ion) battery, reversible heat (RH) makes a considerable contribution to the temperature variation of the battery, and the determination of this contribution is of great significance, especially for mission-critical applications. In previous research works, the determination of including or excluding the RH was typically made based on the rate of discharge. This study, however, finds that the importance of RH could be more meaningfully judged based on its contribution to the overall thermal response of Li-ion battery at various conditions. An improved electrochemical–thermal coupling model is developed to incorporate the RH. This model is applied to simulate the operation of batteries with different physical properties (e.g., electrode thickness and active material particle size) under different discharge rates. The simulation results are compared in terms of RH generation rates, battery temperature, as well as several other associated characteristics. It is found that the significance of RH to the overall heat generation varies when different intrinsic and extrinsic parameters are considered. This significance becomes more appreciable for batteries with thinner electrodes and/or finer active material particles. A correction diagram is then proposed to modify the results for thermal analyses without including RH.

1. Introduction

Lithium-ion (Li-ion) battery system appears to be an effective approach for energy storage and is being applied to address many environmental and economic challenges in modern society. Although numerous innovations have been made in developing new battery materials, such as high capacity loading anode [1], auto shutdown coating and electrolyte [2,3] and high voltage cathode [4], Li-ion technologies have not yet been fully demonstrated to meet the stringent demand from a variety of industries for high-performance batteries. The reliability and safety issues arising from excessive heat generation is being considered as one of the most critical technical challenges inherent to Li-ion battery, which may lead to significant battery performance degradation or even thermal runaway [5], thereby hindering the Li-ion technologies to achieve broader market penetration.

In recent years, many coupling models have been suggested to solve the electrochemical and thermal issues associated with Li-ion battery. For example, Gu et al. [6] coupled an electrochemical battery model with a thermal model. The electrochemical characteristics (in terms of voltage and current density) as well as the thermal characteristics (in terms of heat generation rate and temperature variation under different cooling conditions) were compared between both the coupled and decoupled models, and it was shown that an improved accuracy can be achieved when the thermal model is included. In Ref. [7], the heat generation and

* Corresponding author. Tel.: +1 613 520 2600x8257; fax: +1 613 520 5715.
E-mail address: jliu@mae.carleton.ca (J. Liu).

http://dx.doi.org/10.1016/j.jpowsour.2014.05.034
0378-7753/

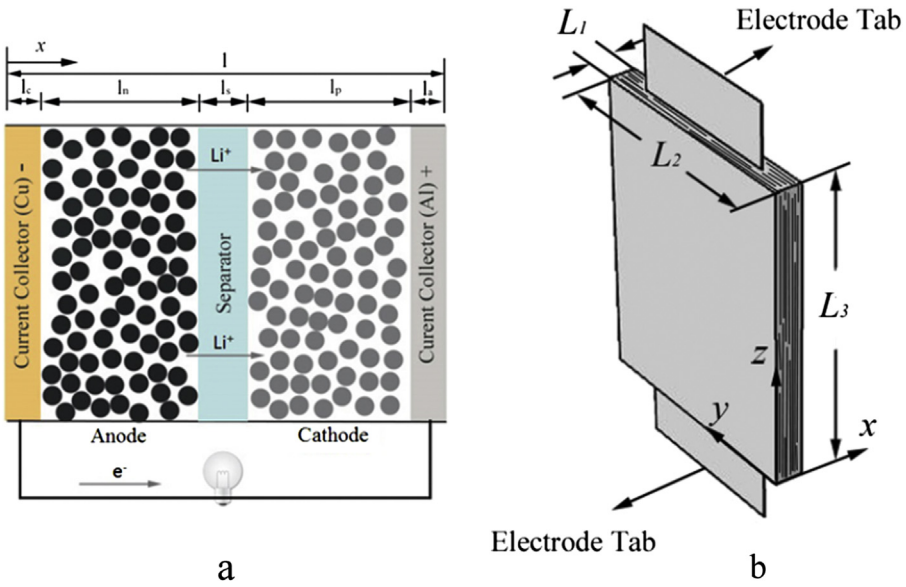

Fig. 1. The schematic illustrations of a) the multi-particle electrochemical reaction cell model; and b) the 3D thermal model of the battery used for validation.

current redistribution in Li-ion battery pack were investigated based on a coupled electrochemical–thermal model considering the contact resistance, and the heat surge from inter-cell connective resistance was discussed. However the effect of the reversible heat (RH) in both models was ignored. RH is also known as the entropy heat and is linked with the entropy changes in the electrodes during the de-intercalation and intercalation processes. In this study, we call the electrochemical–thermal coupling model that does not include RH a "without reversible heat model", or "wor-model". Whether the wor-model can accurately describe the heat generation of a Li-ion battery remains as a challenging technical problem. Therefore, a study was conducted by Srinivasan and Wang [8] on the electrochemical and thermal behaviors of Li-ion battery using two-dimensional unit layer, which indicated that the RH is important at all discharge rates. The experimental results were also provided in the literatures [9–12] for demonstrating the entropy changes in different active materials. Jeon et al. [13] showed the effect of RH to the overall heat generation in Li-ion battery using $LiCoO_2$ and $LiNiCoMnO_2$ as cathodes at different discharge rates when the state of charge equals to 0.1, and it was found that the thermal response of the battery with $LiCoO_2$ cathode has a strong dependence on the RH. We shall call the electrochemical–thermal model with the RH included a "with reversible heat model", or "wr-model". In order to obtain a clearer understanding of the heat generation across the battery, the wr-model will be used in this work. While the previous research works mainly demonstrated the importance of the RH on the entire battery, this study would consider the heat more thoroughly on a component level, with emphasis on the anode and the cathode in an individual reaction cell. Also, unlike the existing literatures that only show the impact of discharge currents on the RH generation, this work takes into consideration many other important electrochemical factors such as the electrode thickness and the active material particle size that may directly or indirectly affect the RH generation.

In this study, the electrochemical and thermal behaviors of $LiMn_2O_4$-based battery are studied using an improved coupling model with the RH term included. By changing the discharge rate, electrode thickness and particle size of active material, the electrochemical and thermal performances of not only the entire battery but also the individual cell components are investigated. For comparison, the simulation results based on a wor-model are also presented. A comprehensive understanding of the significance of the RH in Li-ion battery under various conditions is achieved through in-depth analysis, and a correction diagram that can modify the results for wor-model is thus proposed, which is essential for future research in battery heat generation and battery thermal management system development.

2. Electrochemical–thermal battery model

The fundamental governing equations of the model in this study are mainly based on the model developed by Smith and Wang [14] with some modifications made by including the double layer capacitance term [15] and entropy heat term. The coupling model consists of a 1D electrochemical part and a 3D thermal part, in which the heat generated from the electrochemical part and the temperatures obtained from the thermal part are mutually used as inputs for each other. The schematic of the electrochemical part (i.e., a single reaction cell in lithium ion battery) is shown in Fig. 1a, and all the calculations are performed in the *x* direction.

The 1D electrochemical model has five components from left to right: copper current collector, anode, separator, cathode and aluminum current collector. During discharge, the lithium de-intercalates from the anode particles, resulting in an equal number of Li-ions and electrons at the interface of anode and electrolyte. The Li-ions diffuse through the electrolyte solution and intercalate into the cathode active materials, while the electrons flow through the external circuit from the anode to the cathode to take part in the electrochemical reaction. To mathematically explain the electrochemical reaction and the associated thermal response, equations that describe the mass and charge balances of Li-ions in the electrochemical model as well as the energy conservation in the thermal model should be properly considered.

2.1. 1-D electrochemical model

In the solution phase, the mass balance of Li-ions in the electrolyte is:

$$\varepsilon_e \frac{\partial c_e}{\partial t} = \frac{\partial}{\partial x}\left(D\frac{\partial c_e}{\partial x}\right) + \frac{(1-t_+^0)}{F} j^{\mathrm{Li}} - \left(t_+^0 \frac{d\tilde{q}_-}{d\tilde{q}} - t_-^0 \frac{d\tilde{q}_+}{d\tilde{q}}\right) \frac{t_+^0 a_s C_{\mathrm{dl}}}{F\tilde{v}^+}\left(\frac{\partial \Phi_s}{\partial t} - \frac{\partial \Phi_e}{\partial t}\right) \quad (1)$$

where the last term on the right hand side is the contribution from the double layers, note that $d\tilde{q}_-/d\tilde{q} = 0$ and $d\tilde{q}_+/d\tilde{q} = 1$ for a cation adsorbing electrode and $d\tilde{q}_-/d\tilde{q} = 1$ and $d\tilde{q}_+/d\tilde{q} = 0$ for an anion adsorbing electrode [15].

The solid phase diffusion of the lithium inserted into the active material particle is governed by Fick's second law in the polar coordinate:

$$\frac{\partial c_s}{\partial t} = \frac{D_s}{r^2}\frac{\partial}{\partial r}\left(r^2 \frac{\partial c_s}{\partial r}\right) \quad (2)$$

The current densities in the solid particle ($\mathbf{i_s}$) and in the solution phase ($\mathbf{i_e}$) are given by Ohm's law:

$$\mathbf{i_s} = -\sigma^{\mathrm{eff}} \frac{\partial \Phi_s}{\partial x} \quad (3)$$

$$\mathbf{i_e} = -\left(k^{\mathrm{eff}} \frac{\partial \Phi_e}{\partial x}\right) + \frac{2\mathrm{RT}(1-t_+^0)}{F}\left(k^{\mathrm{eff}} \frac{\partial (\ln c_e)}{\partial x}\right) \quad (4)$$

The relation between the divergence of the current flow in the solution phase and the reaction current density is:

$$\nabla \cdot \mathbf{i_e} = -\frac{n}{s_i} j^{\mathrm{Li}} + a_s C_{\mathrm{dl}}\left(\frac{\partial \Phi_s}{\partial t} - \frac{\partial \Phi_e}{\partial t}\right) \quad (5)$$

The intercalation kinetics in both electrodes can be written in the form of the Bulter–Volmer equation:

$$j^{\mathrm{Li}} = a_s k c_e^{0.5} (c_{s,\max} - c_s)^{0.5} c_s^{0.5}\left[\exp\left(\frac{0.5F}{\mathrm{RT}}\eta\right) - \exp\left(-\frac{0.5F}{\mathrm{RT}}\eta\right)\right] \quad (6)$$

wherein the over-potential η is given by:

$$\eta = \Phi_s - \Phi_e - U \quad (7)$$

where the open circuit potential U of the battery cell is given by Taylor's first order expansion at a reference temperature of 25 °C:

$$U = U_{\mathrm{ref}} + \left(T - T_{\mathrm{ref}}\right)\left(\frac{dU}{dT}\right) \quad (8)$$

and the reference potential U_{ref} of the anode and the cathode at 25 °C in the equation is expressed elsewhere [16]. The entropy change term ($\mathrm{d}U/\mathrm{d}T$) for cathode is expressed as [17]:

$$\frac{dU}{dT} = 4.3128\exp(0.5715\mathrm{y}) + 1.2816\sin(-4.9917\mathrm{y}) - 0.0904\sin(-20.967\mathrm{y} + 12.5788) - 0.03135\sin(31.7663\mathrm{y} - 22.4296) - 4.1453 + 8.1471\mathrm{y} - 26.0646\mathrm{y}^2 + 12.766\mathrm{y}^3 - 0.1843\exp\left(-\frac{\mathrm{y} + 0.5169}{0.04628}\right)^2 \quad (9)$$

and for the anode as [18]:

$$\frac{dU}{dT} = 344.135\frac{\exp(-32.963\mathrm{x} + 8.317)}{1 + 749.076\exp(-34.791\mathrm{x} + 8.887)} + 0.2698 - 0.852\mathrm{x} + 0.362\mathrm{x}^2 \quad (10)$$

where y and x in the Eqs. (9) and (10) denote the ratios of the Li-ion concentrations inside the active materials during cycling and the theoretical maximal concentrations in the cathode and the anode, respectively. The corresponding fits are plotted in Fig. 2.

2.2. 3-D thermal model

Conservation of energy for a Li-ion battery considering convection term and heat generation term can be expressed as:

$$\rho C_p \frac{dT}{dt} = \nabla \cdot (k\nabla T) + q_r + q_{\mathrm{rev}} + q_j \quad (11)$$

where the three "q" s are the volumetric heat generation rate of different heat sources from the electrochemical model, i.e., reaction heat (q_r), reversible heat (q_{rev}) and ohmic heat (q_j):

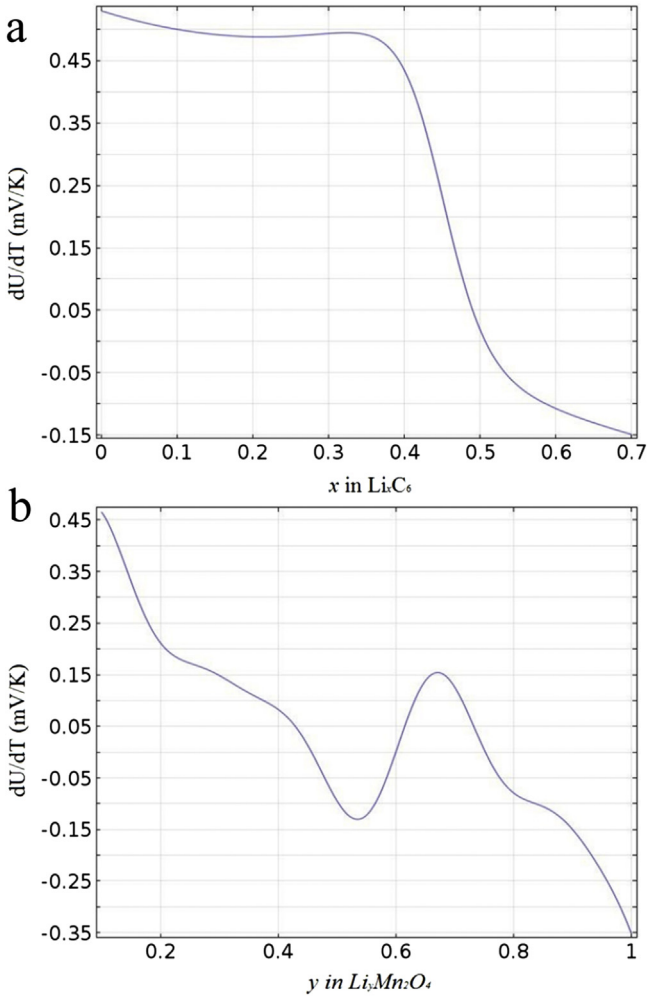

Fig. 2. Fitting curves of the entropy term ($\mathrm{d}U/\mathrm{d}T$) for a) Li_xC_6 from Eq. (10); and b) $Li_yMn_2O_4$ from Eq. (9).

$$q_r = \frac{\int_0^{l_n+l_s+l_p} j^{\mathrm{Li}}(\Phi_s - \Phi_e - U)dx}{l} \quad (12)$$

$$q_{\mathrm{rev}} = \frac{\int_0^{l_n+l_s+l_p} j^{\mathrm{Li}} T \frac{\partial U}{\partial T} dx}{l} \quad (13)$$

$$q_j = \frac{\int_0^{l_n+l_s+l_p} \left[\sigma^{\mathrm{eff}}\left(\frac{\partial \Phi_s}{\partial x}\right)^2 + k^{\mathrm{eff}}\left(\frac{\partial \Phi_e}{\partial x}\right)^2 + \frac{2k^{\mathrm{eff}}\mathrm{RT}}{F}\left(1 - t_+^0\right)\frac{\partial(\ln c_e)}{\partial x}\frac{\partial \Phi_e}{\partial x}\right] dx}{l} \quad (14)$$

where l is the thickness of the five components (anode, separator, cathode and two current collectors) in the cell. In Li-ion battery, each current collector is generally shared by two adjacent reaction cells, therefore the thickness of the current collector used in simulation is half of its actual thickness.

At the surface boundary of the battery, convective cooling is considered:

$$-k\frac{\partial T}{\partial x} = h(T - T_{\mathrm{amb}}) \quad (15)$$

where h refers to the convective coefficient and its value is set as low as 0.1 W m^{-2} k^{-1}. This simulates a condition with a very poor heat transfer rate (e.g., aerospace applications) and can lead to a dramatic temperature rise in batteries, which facilitates a clearer inspection on the differences in temperature elevation between batteries.

The density, heat capacity and thickness of each component are used to determine the average values of the density and heat capacity of the entire battery:

$$\rho C_p = \sum_i \frac{\rho_i C_{p,i} l_i}{L_1} \quad (16)$$

where l_i is the thickness of the component i, and L_1 denotes the thickness of the entire battery. However, the thermal conductivity of the battery should be considered separately in different directions. As suggested by Fig. 1b, there exist series thermal resistors in x direction and parallel thermal resistors in y and z directions, therefore we define:

$$k_x = \frac{\sum_i l_i}{\sum_i \frac{l_i}{k_i}}$$

and

$$k_y = k_z = \sum_i \frac{l_i}{L_1} k_i \quad (17)$$

All the parameters used in the electrochemical and thermal models are listed in Tables 1 and 2, respectively. The l_v and l in Table 2 are the thicknesses of the components in the battery used for validation and in the battery model based on Doyle's work [16], respectively.

3. Results and discussion

Typically, heat generation in Li-ion battery consists of three sources: reversible heat, reaction heat and ohmic heat. Reversible heat (RH), as stated earlier, accounts for the entropy changes in the structure of the electrodes during electrochemical reactions. Reaction heat refers to the heat rises from the reaction current and over-potentials. And ohmic heat is mainly associated with the heat generated during the motion of lithium/lithium-ions in the solid and solution phases. The generation rate of each heat source is related to their respective amount of heat generated in a certain time range, and the contribution of each of them to the overall heat generation gives an indicator of the importance of the heat. With regard to the RH, its generation rate can be related directly to the discharge rate, and its contribution is relied heavily on the amounts of ohmic heat and reaction heat generated, which are found to be

Table 1
Parameters used in the 1D electrochemical model [16].

Parameter	Negative electrode	Separator	Positive electrode
R_s (μm)	12.5	–	8.5
D_s (m^2 s^{-1})	3.9×10^{-14}	–	1×10^{-13}
ε_e	0.357	0.724	0.444
ε_p	0.146	0.276	0.186
ε_f	0.026	0	0.073
$c_{s,\max}$ (mol m^{-3})	26,390	–	22,860
$c_{s,0}$ (mol m^{-3})	14,870	–	3900
c_e (mol m^{-3})	2000	2000	2000
σ (S m^{-1})	100	–	3.8
t_+^0	0.363	0.363	0.363
C_{dl} (F m^{-2})	0.2	–	0.2

Table 2
Parameters used in the 3D thermal model [19–21].

Parameter	Cu foil	Negative electrode	Separator	Positive electrode	Al foil
l_v (μm)	15	37.5	35	24	20
l (μm)	14	100	52	174	20
k (W m^{-1} K^{-1})	398	5	0.334	5	238
ρ (kg m^{-3})	8930	2500	1009	1500	2702
C_p (J kg^{-1} K^{-1})	385	700	1978	700	903

Table 3
Specifications of the $LiMn_2O_4$ battery used for model validation.

Thickness (L_1)	8.6 [mm]
Width (L_2)	115 [mm]
Height (L_3)	140 [mm]
Weight	316 [g]
Nominal voltage	3.7 [V]
Nominal capacity	8.5 [Ah]
Specific energy	100 [Wh kg^{-1}]
Energy density	230 [Wh L^{-1}]
Maximum cut-off charge voltage	4.2 [V]
Minimum cut-off discharge voltage	2 [V]
Charge working temperature	0–40 [°C]
Discharge working temperature	−20 to 55 [°C]

strongly influenced by the electrode thickness and the particle size of active materials, respectively. All of these affecting factors to RH, direct or indirect, will be discussed in details in the following sections.

3.1. Model validation

To validate the proposed model, a discharge test is performed on a commercially available Li-ion battery with a nominal capacity of 8.5 Ah. The other specifications of this type of battery are given in Table 3. In order to prevent heat transfer to the surroundings, a thermally insulated container is employed in the test. Both the experimental battery and the simulated battery go through a galvanostatic discharge process at a 1 C rate (i.e., 8.5 A). The experiment is conducted using a battery analyzer (ESI PCBA 5010-4), and the temperatures of the experimental battery are collected every 60 s by a K-type thermocouple attached at the center of the battery surface. As shown in Fig. 3, the simulation result is well consistent with the data acquired from the experiment, which demonstrates the effectiveness of the coupling model in simulating the thermal response associated with the operation of Li-ion battery.

3.2. Effect of discharge rate

To investigate the influence of discharge rate on the total heat generation and on the proportion that RH accounts for the total heat, simulated discharge processes at rates of 1 C and 4 C are carried out, through which the RH generation rate across battery cell, the total and average heat generation rates with and without RH included, and the corresponding temperature responses are inspected as follows.

Fig. 4 shows the RH generation rate across the cell at 1 C discharge rate, in which the current collectors are not involved since no RH is generated on these two foils. According to Eq. (13), RH can be influenced by the distribution of reaction current density as well as the variation of the entropy term (dU/dT). In the simulation, the cathode is thicker than the anode (Table 2), which makes the distribution of reaction current density is relatively uneven on the cathode. Meanwhile, during the course of discharge, with x in Li_xC_6 decreases from 0.56 to 0.04 and y in $Li_yMn_2O_4$ increases from 0.15 to 0.7, the variation of the entropy term given in Fig. 2

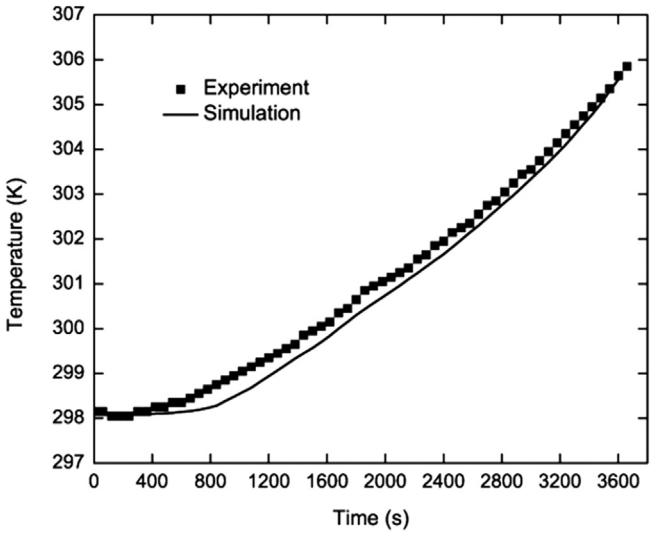

Fig. 3. Comparison of the surface center temperatures obtained from the simulation and experiment at 1 C discharge rate under an adiabatic condition.

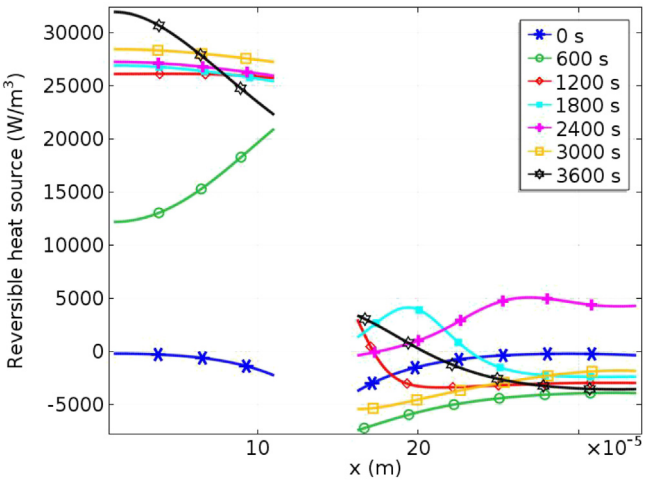

Fig. 4. Reversible heat generation rate across the cell at different depths of 1 C discharge.

fluctuates more on the cathode than that on the anode. As a result, though increases remarkably at the beginning, the RH on the anode remains stable at about 27,000 W m^{-3} during the rest period of discharge, while the variation of RH generation rate at the cathode appears more complex (between −5000 and

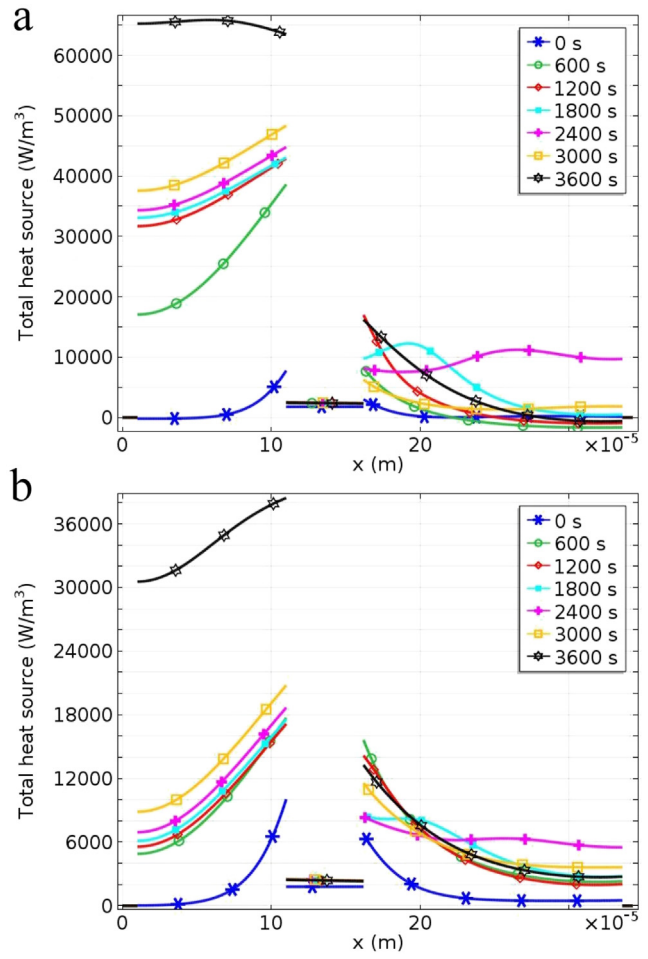

Fig. 5. Total heat generation rates across the cell at different depths of 1 C discharge a) with RH source considered; and b) without RH source considered.

5000 W m^{-3}). And in general, the contribution made by RH to the exothermic behavior of the battery is mainly from the RH generated on the anode.

The total heat generation rate, which differs dramatically for wr-model and wor-model, is also presented across the cell at various depths of discharge (DOD) to identify the contribution that RH made to the total heat. As can be seen from Fig. 5, by including RH, the total heat generation rate at the anode is significantly increased due to the positive RH in this area, with the average values more than twice that of the model neglecting RH at most of the selected DODs. Whereas, the total heat generation at the cathode exhibits a slight decrease after introducing RH for nearly all the chosen time points except 1800 s and 2400 s. The uneven heat distribution across the cell should also be noticed: more heat is generated on the anode and at the interfaces between electrode and separator, which has the potential to cause the active materials close to separator to degrade fast and eventually decreases the reliability of the battery.

Then the average heat generation rates and the temperature curves of the 3D battery models with and without RH included are depicted in Figs. 6a and 7a, respectively. In Fig. 6a, the solid line indicates the heat generation including RH, whereas the dashed line denotes the heat generation excluding RH, and accordingly the difference between these two lines indicates the heat generated from the RH source. When ignoring RH, the average heat generation rate soars in the first few seconds and remains relatively stable at approximately 6000 W m^{-3} for most of the time prior to another increase at the end of discharge, which is believed to be caused by the decrease in the electrolyte salt conductivity that makes the transportation of ions more difficult. In the RH inclusive model, because of the initially negative RH generation rate, the average heat generation rate experiences a moderate increase initially and then a continuous increase until 2500 s when the value of the solid curve is more than twice that of the dashed curve. It eventually drops as a result of the decrease in the RH and the total heat on the cathodes. Correspondingly, in Fig. 7a, the RH inclusive model provides a lower temperature than the RH exclusive model in the beginning of discharge (i.e., 0–800 s), but a faster temperature increase over the rest period of discharge. The temperatures of the battery models with and without RH eventually reach 322.5 K and 311.1 K, respectively. The temperature elevation of the wr-model (24.35 K) almost doubles that of the wor-model (12.95 K).

As the discharge rate increases to 4 C, the RH generation also increases in view of Eq. (13). However, the proportion of RH to the total heat reduces, as indicated by the decreased relative difference between the two lines presented in Fig. 6b compared to Fig. 6a. This is mainly due to the dramatic increase of the ohmic heat which follows an i^2R type of heating scheme. As a result of the reduction of the influence of RH on the overall heat generation across the cell, the temperature elevation caused by RH also becomes less significant. In Fig. 7a, at the end of discharge, though the temperatures increase to as high as 340.8 K and 331.6 K for models with and without RH, respectively, the ratio of the temperature changes ($\Delta T_w/\Delta T_{wo}$), which can reveal the contribution of RH source made to the overall temperature rise, is calculated to be 1.28, far smaller than the 1.88 for the 1 C discharge case.

3.3. Effect of electrode thickness

As a main geometrical parameter of a battery cell, the thickness of electrode can make a big difference in the electrochemical and thermal behaviors of Li-ion battery [22]. Particularly, a variation of the electrode thickness will cause the change of the diffusion distance inside the cell, which can considerably affect the amount of ohmic heat produced, and so do the percentages of different types of heat that constitute the overall heat. In this part, the thickness of the electrochemical reaction unit (including a positive electrode, a negative electrode and their separator) is decreased to 1/4 of the original value while keeping the other parameters constant.

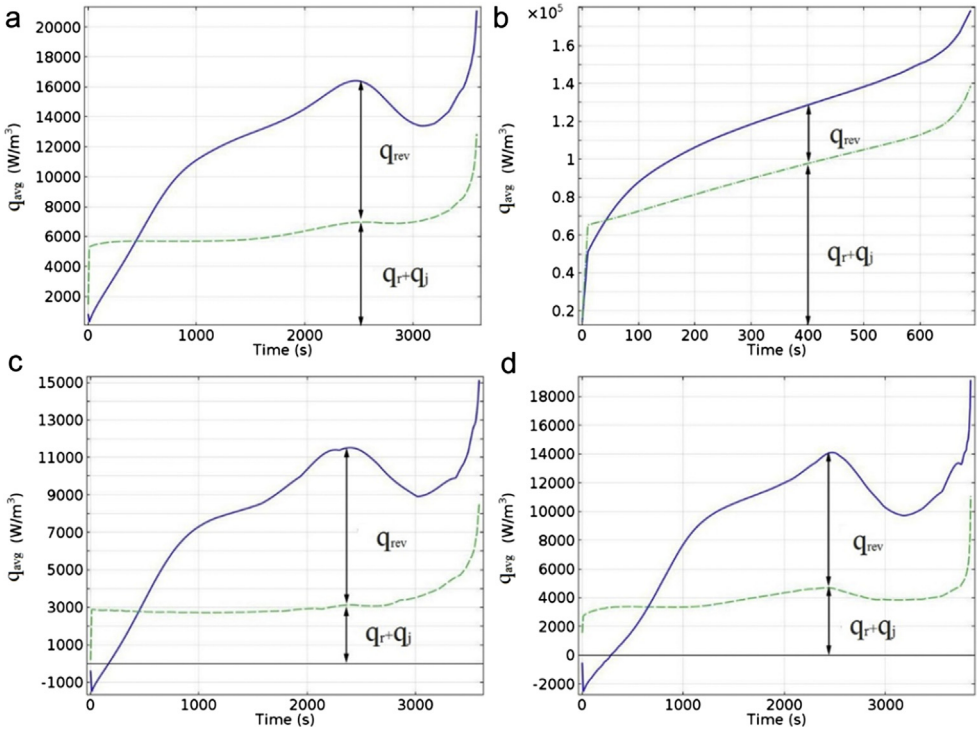

Fig. 6. The average heat generation rates of battery models with (solid line) and without (dashed line) RH included for the a) original cell at 1 C discharge rate, b) original cell at 4 C discharge rate, c) cell with thin electrode at 1 C discharge rate, d) cell with small particle size at 1 C discharge rate.

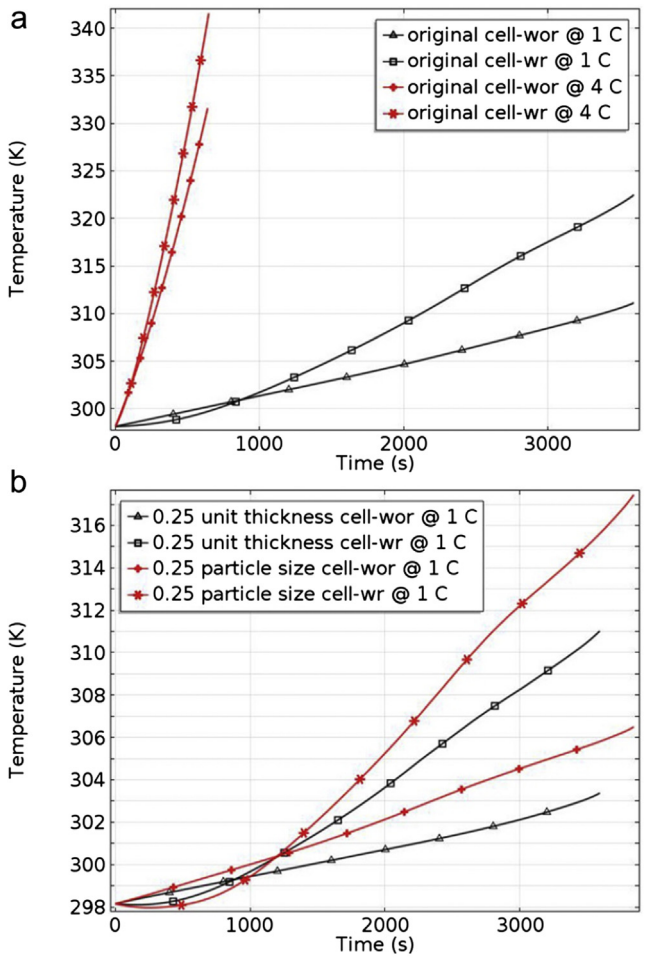

Fig. 7. Temperature curves of the models with/without RH included for a) original cell discharged at 1 C and 4 C rates; and b) adjusted cells discharged at 1 C rate.

Considering the current applied on the current collector is proportional to the thickness of the electrode, it decreases as the same rate as the electrode thickness, i.e., from 17.5 A m^{-2} to 3.75 A m^{-2} for the 1 C discharge rate. In order to obtain the same capacity as the original battery, 3 times more reaction cells are needed. Overall, the thickness of the newly built 3D thin-electrode battery thermal model is 1.15 times of that of the original model.

Fig. 8 shows the RH generation rate across the adjusted cell at assigned DODs. Although the applied current decreases, the reaction current density in each cell remains unchanged owing to the decreased electrode thickness, as evidenced by the similar RH generation rate across the cell before and after changing the electrode thickness.

The total heat generation rates of the RH inclusive and exclusive models are given in Fig. 9a and b, respectively. As the electrode thickness decreases, the total heat distribution across the cell exhibits an improved uniformity, which can benefit the long-term performance and stability of Li-ion battery. The explanation of the improved uniformity is that during the operation of the Li-ion battery, the movement of lithium ions, driven by the potential and concentration gradients, both in the electrolyte and in the active particle materials, is the limited step (slower than the transportation of electrons). Therefore the decrease in the diffusion distance can facilitate the electrochemical reactions and hence produces a better distributed current and reaction depth, a reduced concentration polarization, a less ohmic heat generation and finally promotes a more even heat distribution across the battery cell. Furthermore, due to the decrease of the ohmic heat, the proportion of RH to the overall heat increases, as is evident from the comparison made between Figs. 9 and 5.

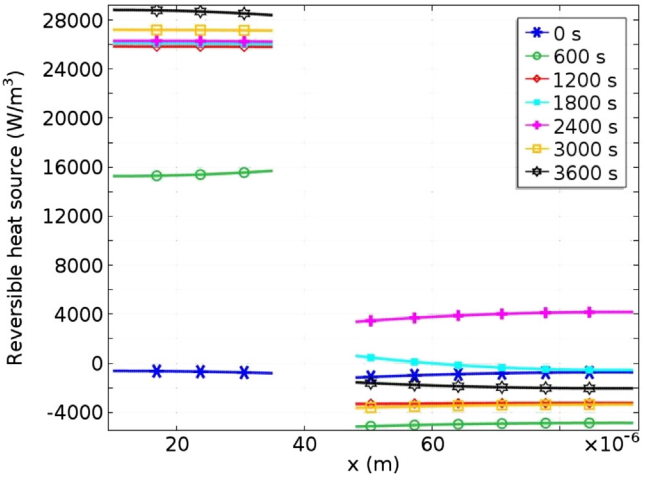

Fig. 8. Reversible heat generation rate across the cell with thin electrodes at different depths of 1 C discharge.

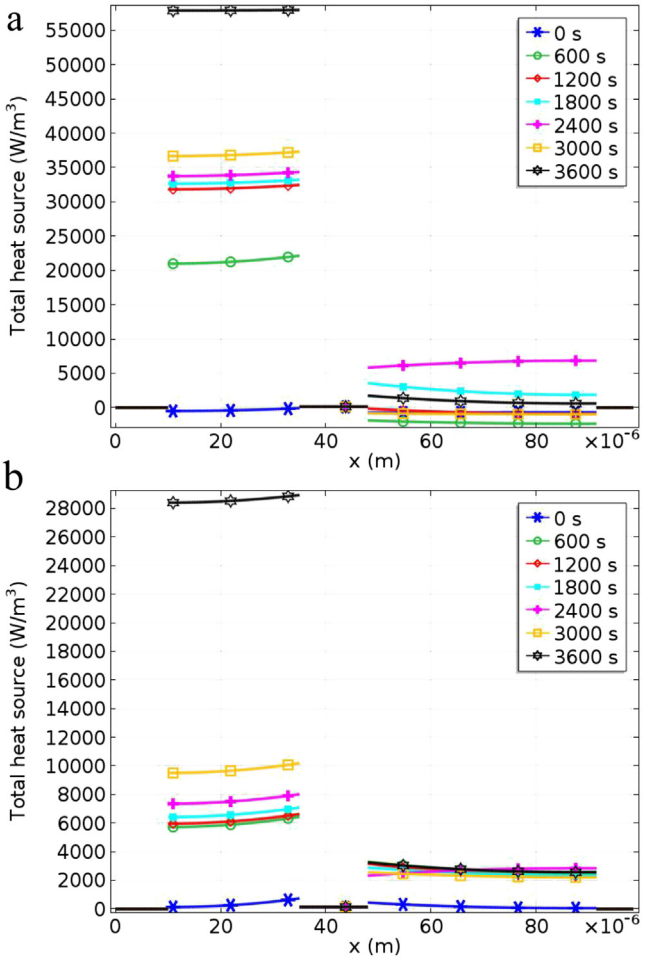

Fig. 9. Total heat generation rates across the cell with thin electrodes at different depths of 1 C discharge a) with RH source considered; and b) without RH source considered.

Different from previous models, the average heat generation rate of the thin-electrode battery wr-model (see Fig. 6c) experiences a sudden drop at the very beginning of discharge, which is the combined effect of the decreased ohmic heat and the negative reversible heat, and at 2500 s, the heat generation rate of the wr-model increases to almost 4 times that of the wor-model. From the big difference of the heat generation rates of the wr-mode and the wor-model, the significance of RH to the heat generation of the battery with thin electrodes can be recognized.

In Fig. 7b, an alleviated temperature elevation can be observed in the battery with adjusted electrode thickness. Compared to the original battery, the final temperature of the wr-model decreases from 322.5 K to 311 K, which not only reduces the security risks but also enhances the well-being and cycle life of the battery. Meanwhile, the ratio of the temperature elevations of the wr-model and wor-model becomes significantly bigger in the adjusted battery, 2.45, than in the original battery, 1.88. In light of the large ratio, it is fair to conclude that the temperature response of the battery will be substantially undervalued by excluding RH from the simulation, especially for the battery with thin electrochemical reaction cells.

3.4. Effect of active material particle size

The solid particle size of electrode active materials has also been acknowledged as an important factor affecting the electrochemical processes inside the Li-ion battery [23,24]. The decrease in particle size can facilitate and accelerate the processes of de-intercalation and intercalation, and therefore changes the time and depth of the electrochemical reactions taking place inside the battery during discharge. In order to investigate the influence of particle size on the thermal behavior of the battery, in this part, active materials with 1/4 of the original particle size for both anode and cathode are used, with all the other parameters remain the same. Also, the adjusted cell with the new particle size undergoes a 1 C discharge process.

Prior to the analysis of thermal behavior, a comparison made between the discharge curves of the battery models before and after modifying particle size is conducted. As depicted in Fig. 10, the discharge process lasts longer in the battery with smaller particles, which allows a better utilization of active materials and hence provides a higher capacity output, 18.7 Ah m^{-2}, as compared to the 17.5 Ah m^{-2} of the original battery. The explanation is based on two aspects: first, in battery with smaller particle size, the difference between the Li-ion concentration at the surface and in the center of the electrode particle is smaller due to the shorter diffusion distances for both de-intercalation and intercalation reactions; second, during discharge, the Li-ions diffuse from the center of the anode particles to the surface to react, and once the surface Li-ion concentration drops to zero, the reactions stop. Combining these two aspects, at any time point, the Li-ion concentration at the surface of the original anode particles is lower than that of the small particles due to the longer diffusion distance. And eventually, due to the lack of Li-ion supply on the anode surface, the electrochemical reactions in the original battery suffer an early stop.

Fig. 11 outlines the RH generation rate across the reaction cell with modified particle size at assigned DODs. Comparing with Fig. 4 (RH of the original cell), the decrease in particle size has almost no direct impact on the amount of the RH generated except promoting a faster response and a better material utilization, as is suggested by the intensive endothermic behavior at the interfaces between electrodes and separator at 0 s. And at any time point, the difference in diffusion distance results in the x in Li_xC_6 lower in the original particle than in the adjusted particle, and thereby, as indicated in Fig. 2, the RH of original cell always corresponds to a time point that is ahead of the time point to which the RH of new cell corresponds. At 3600 s, the RH across the anode maintains stable at approximately 28,000 W m^{-3} in the newly built cell, whereas it distributes unevenly in the original cell with a variation of 10,000 W m^{-3} (from 24,000 to 34,000 W m^{-3}), which is attributed to the non-uniform reaction current distribution on the anode as well as the uneven utilization of active materials.

The active material particle size is related directly to the generation of reaction heat, which is less produced from the reaction over-potential since with finer particle size the de-intercalation/intercalation reactions in the battery become more fluent. Fig. 12 presents the reaction heat generation of the models with original and decreased particle sizes. As shown, the reaction heat of the anode stays at around 7000 W m^{-3} during the stable stage of discharge in the original cell, while it reduces to only about 1700 W m^{-3} for the cell with smaller particle size, which is almost 3/4 less, and the change is basically proportional to the particle size.

As a consequence, similar to the case of thin-electrode model, the average heat in the model with small active material particle has a higher dependency on RH than in the original one, with the proportion of RH to total heat at 2500 s of 67.6%. Moreover, as is

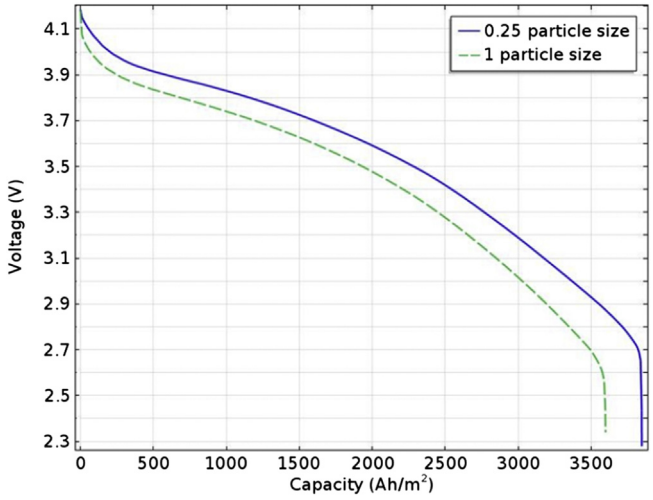

Fig. 10. Discharge curves of the battery models with original particle size (dashed line) and 1/4 of the original particle size (solid line).

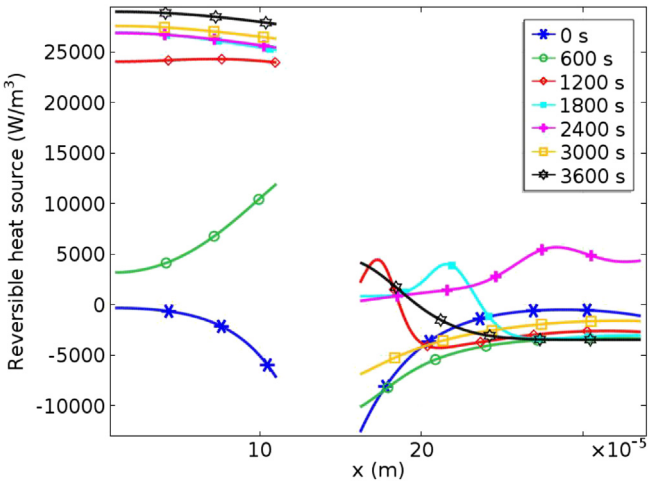

Fig. 11. Reversible heat generation rate across the cell with small particles at different depths of 1 C discharge.

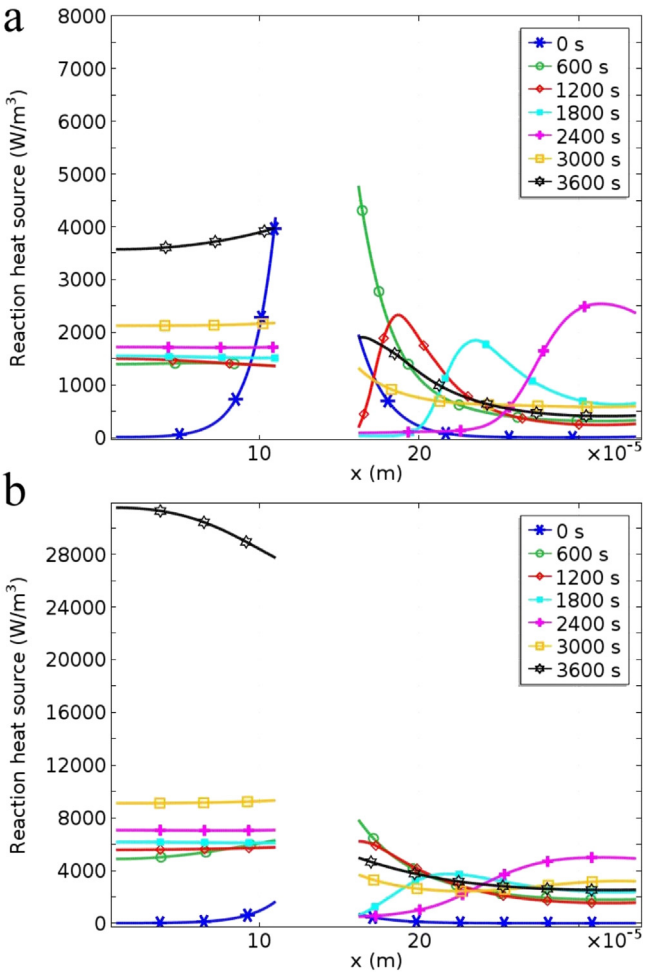

Fig. 12. Reaction heat generation rate across the cell at different DODs when a) 1/4 of the original particle size and b) original particle size are used.

represented in Fig. 7b, the temperature curves for the small-particle model have similar trends as those for the thin-electrode model, with the final temperatures grows higher to 317.5 K ($\Delta T = 19.35$ K) and 306.5 K ($\Delta T = 8.35$ K) for wr-model and wor-model, respectively. The big ratio of the temperature elevations once again proves the significance of taking the RH into consideration, this time for cells using small particle size.

To give a brief summary, all the adjusted parameters and the associated results are listed in Table 4. The decreased final temperatures for the thin-electrode battery and for the small-particle battery illustrate an improvement in the thermal performance of these batteries with respect to the original cell under 1 C discharge rate. Note that the high temperature of the original battery discharged at 4 C rate should be properly managed, either in a passive way [25] or in an active way [26], otherwise it can degrade the performance and reliability of Li-ion battery, or even bring about

Table 4
Summary of the parameter-varying models and the results related to the effect of reversible heat.

Model	C-rate	l/l_0	R/R_s	q_{rev}% at DOD = 0.7	$\Delta T_w/\Delta T_{wo}$	T_{final} (K)
1	1	1	1	57.6	1.88	322.5
2	4	1	1	24.7	1.28	340.8
3	1	0.25	1	72.6	2.45	311
4	1	1	0.25	67.6	2.32	317.5

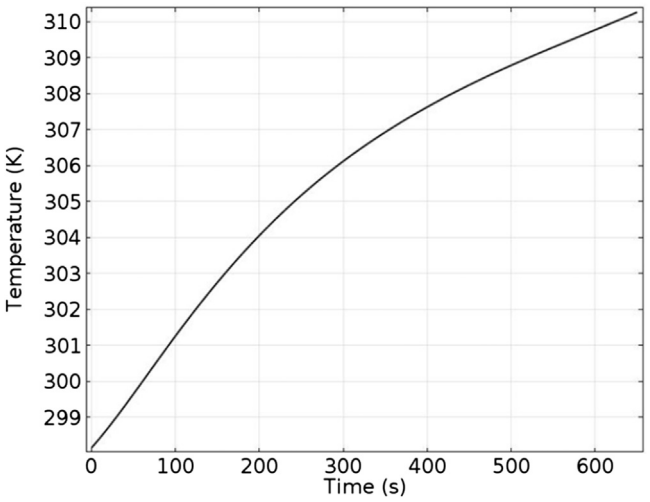

Fig. 13. Simulated temperature curve of the original battery at 4 C rate with forced air convective cooling.

safety issues, such as thermal runaway. One of the most commonly used active cooling approaches, forced air cooling method, has been adopted in the simulation to control the temperature rise of the original battery discharged at a 4 C rate, with a convective coefficient value of 40 W m^{-2} K^{-1}. The simulation results are shown in Fig. 13. As can be seen, the maximum temperature decreases from 340.8 K to 310.2 K when the forced air convective cooling is applied.

Fig. 14 indicates the combined effects of the *C*-rate (1, 2, 4, 6, 8, 10 C) and the electrode thickness (0.1, 0.2, 0.4, 0.6, 0.8, 1 of the original cell) on the results of $\Delta T_w/\Delta T_{wo}$ (due to the similar effects of the electrode thickness and the particle size on thermal response, the figure associated with the impact from particle size is not provided here). The projections of the obtained data points are depicted on the two vertical surfaces, which give the variation trend of the ratio of the temperature rise with respect to the *C*-rate and the relative thickness. The big ratios shown in the figure reveal that the battery with thin electrodes and/or discharging at low *C*-

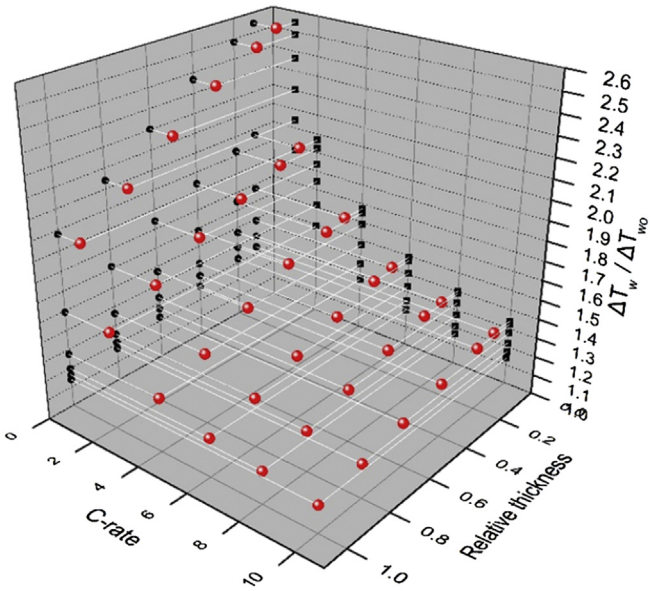

Fig. 14. Combined effects of electrode thickness and discharge rate on the ratio of temperature elevations in models including and excluding reversible heat.

rates can produce significant proportion of RH to the total heat, and although this proportion decreases as the electrodes become thicker and/or the discharge rate becomes higher, the contribution of RH should be taken into account for discharge processes at 10 C or lower rates. Furthermore, this diagram is expected to be used for correcting the final temperatures obtained in the previous and future thermal analyses of Li-ion batteries that do not include the reversible heat.

4. Conclusion

In this paper, a reversible-heat-included Li-ion battery model consisting of a 1D electrochemical part and a 3D thermal part is developed and used to simulate several galvanostatic discharge processes on batteries with different physical properties. By comparing the results obtained from the wr-model and from the wor-model, a better understanding of the importance of RH to the overall thermal performance of Li-ion battery under different conditions is achieved, based on which a correction diagram is proposed to modify the results for the thermal analyses on Li-ion batteries that do not include RH at first.

RH is non-ignorable in battery discharged at low rates, but its contribution to the total heat decreases as a result of the dramatic increase of the ohmic heat at high rates. Battery with thinner electrodes relies heavier on the RH than that with thicker electrodes. Instead of the change of the RH itself with the reduction of the thicknesses of electrodes, the considerable decrease in ohmic heat generation takes the main responsibility, which indirectly increases the contribution of RH to the total heat generation. Similarly, the effect of RH is greater in battery with smaller active material particle size, as a result of the decreased reaction heat.

Moreover, a strong correlation between the battery temperature and the battery cell characteristics is demonstrated. It is shown that the decrease in any of these two parameters, i.e., electrode thickness and active material particle size, can reduce the battery temperature during operation and thereby improving the performance, reliability and even safety of Li-ion battery.

Overall, the significance analysis of reversible heat is crucial when precise information about the heat generation and the heat distribution across a battery cell is demanded and should be conducted case-by-case since the proportion of RH varies dramatically with the applied currents and with the characteristics of the electrochemical battery under study.

Acknowledgment

The financial support by the Ontario China Research and Innovation Fund is gratefully acknowledged. The valuable comments and suggestions from the anonymous reviewers would also be much appreciated.

Nomenclature

a_s	active surface area per electrode unit volume, $cm^2\ cm^{-3}$
c	volume-averaged concentration of lithium in a phase, mol cm^{-3}
$c_{s,max}$	maximum concentration of lithium in solid phase, mol cm^{-3}
$c_{s,0}$	initial concentration of lithium in solid phase, mol cm^{-3}
C_{dl}	double layer capacitance, F m^{-2}
C_p	specific heat capacity of component inside cell, J kg^{-1} K^{-1}
D	diffusion coefficient of lithium species, cm^2 s
D_s	diffusion coefficient of lithium in the electrode particles, cm^2 s
e^-	electrons
F	Faraday's constant, 96,487 C mol^{-1}
h	convective heat transfer coefficient, W m^{-2} K^{-1}
$\mathbf{i_e}$	solution phase current density, A cm^{-2}
$\mathbf{i_s}$	solid phase current density, A cm^{-2}
j^{Li}	reaction current density, A cm^{-3}
k	conductivity of different components inside cell, W m^{-1} K^{-1}
k^{eff}	effective electrolyte conductivity, S m^{-1}
l_c	thickness of copper foil, cm
l_n	thickness of negative electrode, cm
l_s	thickness of separator, cm
l_p	thickness of positive electrode, cm
l_a	thickness of aluminum foil, cm
l_v	thickness of components in experimental cell, cm
l	thickness of entire electrochemical cell, cm
L_1	thickness of experimental battery, cm
L_2	width of experimental battery, cm
L_3	length of experimental battery, cm
n	number of electrons transferred in the electrode reaction
q	heat generation rate, W m^{-3}
q_r	reaction heat generation rate, W m^{-3}
q_{rev}	reversible heat generation rate, W m^{-3}
q_j	ohmic heat generation rate, W m^{-3}
$\tilde{q}$	charge density on the double layer surface, C m^{-2}
r	radial coordinate along active material particle, cm
R	universal gas constant, 8.3143 J mol^{-1} K^{-1}
s_i	stoichiometric coefficient
t	time, s
t^0	transference number
T	temperature, K
U	open circuit potential, V
dU/dT	entropy change term, mV K^{-1}
U_{ref}	open-circuit potential of an electrode reaction, V
x	x coordinate
x	negative electrode solid phase stoichiometry
y	y coordinate
y	positive electrode solid phase stoichiometry
z	z coordinate

Greek symbols

ε	volume fraction or porosity of a phase
η	surface over-potential of an electrode reaction, V
κ	reaction rate constant
σ	conductivity of solid active materials in an electrode, S cm^{-1}
ρ	density of the battery, kg m^{-3}
$\tilde{\nu}^+$	number of cations of anions into which a mole of electrolyte dissociates
Φ	electrical potential in a phase, V

Subscripts

amb	ambient
c	convection
e	electrolyte phase
f	conductive filler additive
i	ith component
p	polymer phase
ref	with respect to a reference state
s	solid phase

Superscripts

eff	effective value

References

[1] H. Li, X. Huang, L. Chen, Z. Wu, Y. Liang, Electrochem. Solid-State Lett. 2 (1999) 547–549.
[2] C.C. Lin, H.C. Wu, J.P. Pan, C.Y. Su, T.H. Wang, H.S. Sheu, N.L. Wu, Electrochim. Acta 101 (2013) 11–17.
[3] L. Xia, D. Wang, H. Yang, Y. Cao, X. Ai, Electrochem. Commun. 25 (2012) 98–100.
[4] H. Kawai, M. Nagata, H. Tukamoto, A.N. West, J. Power Sources 81–82 (1999) 67–72.
[5] T.M. Bandhauer, S. Garimella, T.F. Fuller, J. Electrochem. Soc. 158 (2011) R1–R25.
[6] W.B. Gu, C.Y. Wang, ECS Proc. 99 (25) (2000) 748–762.
[7] B. Wu, V. Yufit, M. Marinescu, G.J. Offer, R.F. Martinez-Botas, N.P. Brandon, J. Power Sources 243 (2013) 544–554.
[8] V. Srinivasan, C.Y. Wang, J. Electrochem. Soc. 150 (2003) A98–A106.
[9] Y. Reynier, J. Graetz, T. Swan-Wood, P. Rez, R. Yazami, B. Fultz, Phys. Rev. B 70 (2004) 174304.
[10] Y. Reynier, R. Yazami, B. Fultz, J. Electrochem. Soc. 151 (2004) A422–A426.
[11] S.W. Kim, S.I. Pyun, Electrochim. Acta 46 (2001) 987–997.
[12] R. Williford, V. Viswanathan, J.G. Zhang, J. Power Sources 189 (2009) 101–107.
[13] D.H. Jeon, S.M. Baek, Energy Convers. Manage. 52 (2011) 2973–2981.
[14] K. Smith, C.Y. Wang, J. Power Sources 160 (2006) 662–673.
[15] G. Sikha, R.E. White, B.N. Popov, J. Electrochem. Soc. 152 (2005) A1682–A1693.
[16] M. Doyle, J. Newman, A.S. Gozdz, C.N. Schmutz, J.M. Tarascon, J. Electrochem. Soc. 143 (1996) 1890–1903.
[17] K.E. Thomas, C. Boguta, J. Newman, J. Electrochem. Soc. 148 (2001) A570–A575.
[18] S. Al Hallaj, R. Venkatachalapathy, J. Prakash, J.R. Selman, J. Electrochem. Soc. 147 (2000) 2432–2436.
[19] P. Taheri, M. Yazdanpour, M. Bahrami, J. Power Sources 243 (2013) 280–289.
[20] S.C. Chen, C.C. Wan, Y.Y. Wang, J. Power Sources 140 (2005) 111–124.
[21] U.S. Kim, C.B. Shin, C.S. Kim, J. Power Sources 189 (2009) 841–846.
[22] H. Zheng, J. Li, X. Song, G. Liu, V.S. Battaglia, Electrochim. Acta 71 (2012) 258–265.
[23] C.H. Lu, S.W. Lin, J. Power Sources 97–98 (2001) 458–460.
[24] Y. Chen, K. Xie, Y. Pan, C. Zheng, J. Power Sources 196 (2011) 6493–6497.
[25] R. Zhao, S. Zhang, J. Gu, J. Liu, S. Carkner, E. Lanoue, J. Power Sources 255 (2014) 29–36.
[26] H. Park, J. Power Sources 239 (2013) 30–36.